ANATOMY-GUIDED BRAIN PET IMAGING INCORPORATING A JOINT PRIOR MODEL

Lijun Lu[1], *Jianhua Ma*[1], *Jing Tang*[2], *Qianjin Feng*[1], *Arman Rahmim*[3, 4] and *Wufan Chen*[1]

[1]School of Biomedical Engineering, Southern Medical University, Guangzhou, Guangdong 510515, China
[2]Department of Electrical& Computer Engineering, Oakland University, MI 48309, USA
[3]Department of Radiology, Johns Hopkins University, Baltimore, MD 21287, USA
[4]Department of Electrical & Computer Engineering, Johns Hopkins University, Baltimore, MD 21218, USA

ABSTRACT

We proposed a maximum a *posterior* (MAP) framework for incorporating information from co-registered anatomical images into PET image reconstruction through a novel anato-functional joint prior. The characteristic of the utilized hyperbolic potential function is determinate by the voxel intensity differences within the anatomical image, while the penalization is computed based on voxel intensity differences in reconstructed PET images. Using realistic simulated short time ^{18}FDG PET scan data, we optimized the performance of the proposed MAP reconstruction with the joint prior (JP-MAP), and compared its performance with conventional 3D maximum likelihood expectation maximization (MLEM) and MAP reconstructions. The proposed JP-MAP reconstruction algorithm resulted in quantitatively enhanced reconstructed images, as demonstrated in extensive ^{18}FDG PET simulation study.

Index Terms—positron emission tomography, maximum a *posterior,* anatomical priors, joint prior

1. INTRODUCTION

Positron emission tomography (PET) is a powerful molecular imaging modality enabling quantitative measurements of physiological and biochemical process in vivo. However, the quantitative accuracy of PET imaging is limited by several factors including the intrinsic resolution of the imaging system and inherently noisy data [1]. The incorporation of anatomical information into the Bayesian PET reconstruction can potentially improve the quality of PET images [2]. Some approaches seek to control regularization (e.g. quadratic penalty or prior) by preventing the smoothing across anatomical boundaries to avoid activity spillover between distinct regions [3]. Others seek to encourage a homogeneous distribution of tracers within each anatomical region [4]. Nevertheless, these techniques rely on the explicit boundary or regional information derived from anatomical image by segmentation or edge detection.

Bowsher et al [5] proposed an anatomical prior avoiding use of segmented anatomical information. This prior (referred to as the Bowsher prior) encourages smoothing over an anatomy-dependent neighborhood, defined by selecting a set of most similar neighbors in the anatomical image [6]. Some generalization of Bowsher prior also has been proposed [7, 8]. Overall, all these methods try to modify the weight of the potential function (commonly quadratic function) based on the anatomical information rather than the PET image itself. More recent work has tended to apply no segmentation of the anatomy but involve information-based similarity measure priors in the literature [9-12].

By contrast, the present work investigates a straight-forward hyperbolic potential function employing non-segmentation anatomical information to enhance the PET image reconstruction. The characteristic of the potential function is determinate by the voxel intensity differences in the anatomical image, while the penalization is computed based on voxel intensity differences in the PET images. We have designed a one-step-late (OSL) maximum a *posteriori* (MAP) algorithm incorporating the anatomical information via the joint prior. The performance of the proposed techniques was evaluated in terms of regional and overall noise versus bias using realistic HRRT brain imaging.

2. METHODS

2.1. MAP PET image reconstruction

Let $\mathbf{f}=\{f_j\}$ denote the unknown emission distribution. The PET data $\mathbf{g}=\{g_i\}$, modeled as a collection of independent Poisson random variables with expectation $\bar{\mathbf{g}}=\{\bar{g}_i\}$, can be related to $\mathbf{f}$ through an affine transform:

This work was supported by the 973 Program of China under grant no. 2010CB73250, NIH grant 1S10RR023623, the Specialized Research Fund for the Doctoral Program of Higher Education under grant 20134433120017 and the National Natural Science Foundation of China under grants 81371544 and 81101046.
Corresponding author: W. Chen (e-mail: chenwf@fimmu.com).

$$\bar{\mathbf{g}}(\mathbf{f}) = \mathbf{P}\mathbf{f} + \mathbf{r}, \tag{1}$$

where $\mathbf{P} \in R^{n_i \times n_j}$ is the system matrix with element p_{ij} denoting the element, $\mathbf{r} \in R^{n_i}$ accounts for the scattered and random events, and n_i and n_j denote the total number of detector pairs and voxels, respectively.

According to the measurement model, the log-likelihood function of the measured data is given by

$$L(\mathbf{g} \mid \mathbf{f}) = \sum_{i=1}^{n_i} g_i \log \bar{g}_i(\mathbf{f}) - \bar{g}_i(\mathbf{f}), \tag{2}$$

where $\mathbf{g}$ and $\mathbf{f}$ denote the measured sinograms and the unknown emission distributions, respectively.

Commonly, the prior is modeled to follows a Gibbs distribution [13]:

$$P(\mathbf{f}) \propto \exp\{-\beta U(\mathbf{f})\}, \tag{3}$$

where $U(\mathbf{f})$ is the energy function and β is a regularization parameter that controls the tradeoff between resolution and noise. Combining the likelihood function and the image prior, MAP estimation of $\mathbf{f}$ is given by

$$\hat{\mathbf{f}} = \arg\max_{\mathbf{f} \geq \mathbf{0}} \{L(\mathbf{g} \mid \mathbf{f}) - \beta U(\mathbf{f})\}. \tag{4}$$

Based on equations (2) and (4), we then invoke the one-step-late (OSL) approach for an iterative update to the MAP estimate [14]:

$$f_j^{new} = \frac{f_j^{old}}{\sum_i p_{ij} + \beta \frac{\partial U(\mathbf{f})}{\partial f_j}\Big|_{f_j = f_j^{old}}} \sum_i \frac{p_{ij} g_i}{\sum_j p_{ij} f_j^{old} + r_i}, \tag{5}$$

where the new estimate of voxel j is updated from the old estimate. A single bin i of the measured sinogram $\mathbf{g}$ is represented by g_i, and p_{ij} represents an element of the system matrix $\mathbf{P}$. β is the regularization parameter.

2.2. The proposed joint prior model

Assume that the PET image $\mathbf{f}$ and the anatomical image $\mathbf{a}$ are very well registered. If neighboring voxel values in the anatomical image $\mathbf{a}$ are similar, the corresponding voxels in the PET image are more likely to belong to the same organ or region. Thus, we define a joint prior that includes both the anatomical and functional information:

$$U(\mathbf{f}, \mathbf{a}) = \sum_{j=1}^{n_j} \sum_{k \in N_j} w_{kj} v(f_j, f_k, a_j, a_k), \tag{6}$$

where w_{kj} is the weight of a given voxel k in the neighborhood of voxel j, and

$$v(f_j, f_k, a_j, a_k) = \sqrt{1 + \left(\frac{f_j - f_k}{\delta}\right)^2 + \left(\frac{a_j - a_k}{\eta}\right)^2} - 1. \tag{7}$$

δ and η are adjustable parameter in the joint prior model. To illustrate how this encourages smoothness in portions of the PET image where the anatomical image is smooth, consider the partial derivative of joint potential function in terms of the difference in voxel values

$$\frac{\partial v(\Delta f_{jk}, \Delta a_{j_k})}{\partial \Delta f_{jk}} = \frac{\delta^{-2} \Delta f_{jk}}{\sqrt{1 + \left(\frac{\Delta f_{jk}}{\delta}\right)^2 + \left(\frac{\Delta a_{jk}}{\eta}\right)^2}}. \tag{8}$$

where $\Delta f_{jk} = f_j - f_k$ and $\Delta a_{jk} = a_j - a_k$.

Fig. 1 plots the derivative of the potential function for several different values of Δa_{jk} where δ and η are 1. Note that the "force" increases more rapidly as a function of the difference in the voxel values in the PET image $\mathbf{f}$ when the difference in the voxel values in the anatomical image $\mathbf{a}$ is smaller.

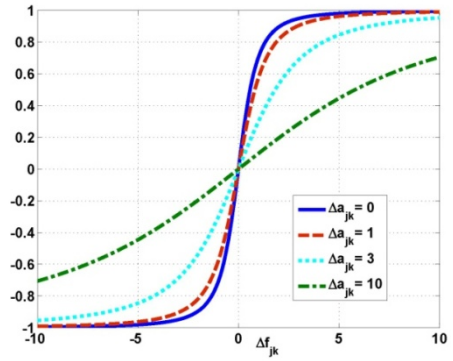

Fig. 1. Plots of the derivative of the potential function for several different values of Δa_{jk} where δ and η are 1.

3. EXPERIMENTAL DESIGN

We performed realistic analytic simulations for the geometry of the high resolution research tomography (HRRT) [15], a dedicated-brain 3D-only acquisition system. Decay, normalization and attenuation effects were taken into account; these effects were also incorporated within the reconstructions. A mathematical human brain phantom was used for the purpose of performing realistic brain tomography imaging [16]. The PET activities in the various regions of the brain were specified based on a 2 minutes clinical FDG study. Additionally, a corresponding MRI image was generated based on a patient MRI intensity measurement. All images were reconstructed with matrix dimensions of $256 \times 256 \times 207$ and cubic voxel sizes of $1.219 \times 1.219 \times 1.219$ mm^3.

Figures of Merit (FOMs): To compare the images reconstructed from the different algorithms described in the previous subsection, we used quantitative evaluation criteria involving regional normalized standard deviation (NSD) versus bias tradeoff curves. We studied ten regions of interest (ROIs). The normalized standard deviation (NSD_{ROI}) for each ROI was defined as in [17]

$$\mathrm{NSD}_{\mathrm{ROI}}=\frac{\sqrt{\frac{1}{N_{\mathrm{ROI}}-1}\sum_{j\in\mathrm{ROI}}\left(X_j-\bar{X}_{\mathrm{ROI}}\right)^2}}{\bar{X}_{\mathrm{ROI}}}\times 100\%, \qquad (9)$$

where X_j denotes the reconstructed PET image value at a voxel j ($j=1,...,N_{\mathrm{ROI}}$) of the specified ROI, and $\bar{X}_{\mathrm{ROI}}=\frac{1}{N_{\mathrm{ROI}}}\sum_{j\in\mathrm{ROI}}X_j$ represents the mean value of reconstructed PET image value in a specified ROI. For a given ROI of known uniform PET image value $X_{\mathrm{ROI}}^{\mathrm{true}}$, the regional bias ($\mathrm{Bias}_{\mathrm{ROI}}$) was defined as

$$\mathrm{Bias}_{\mathrm{ROI}}=\frac{\left|\bar{X}_{\mathrm{ROI}}-X_{\mathrm{ROI}}^{\mathrm{true}}\right|}{X_{\mathrm{ROI}}^{\mathrm{true}}}\times 100\%. \qquad (10)$$

Overall FOMs: To quantify $\mathrm{NSD}_{\mathrm{overall}}$ versus $\mathrm{Bias}_{\mathrm{overall}}$ for the entire image (in order to allow an overall assessment of quantitative performance), $\mathrm{NSD}_{\mathrm{ROI}}$ and $\mathrm{Bias}_{\mathrm{ROI}}$ values for the ROIs (r=1, 2, …, R) were averaged, and weighted by the size (number of voxels N_{ROI}) for each ROI to estimate the overall NSD and Bias.

4. RESULTS

We evaluated the proposed MAP reconstruction (JP-MAP) algorithm in comparison MLEM and MAP (using single hyperbolic prior, SP-MAP) reconstruction algorithms. First, the effect of varying the parameter δ in the hyperbolic potential function was studied. This was achieved using noise versus bias tradeoff curves (not shown). We utilized $\delta^{1/2}=150$ as an optimal value for SP-MAP and proposed JP-MAP reconstructions. Next, with the optimized δ and fixed β, we optimized the parameter η in terms of overall noise versus bias tradeoff (not shown). We utilized 100 as the optimal value for proposed JP-MAP reconstruction. With the optimized δ and η, we optimized the regularization β in terms of overall noise versus bias tradeoff (shown in Fig. 2). For the β -values plotted, considerable improvements in image quality were achieved when β increased from 0.01 to 0.2 (increasing β to 0.5 did not much further reduce the NSD value, while adversely impacting bias). We thus utilized $\beta=0.2$ as an optimal value for JP-MAP reconstructions.

Following the optimization of parameters, we compared the performance of conventional 3D PET reconstruction (including MLEM, SP-MAP) and proposed MAP reconstruction (JP-MAP). We take 10 iterations with 16 subsets for all reconstruction approaches in performance comparison. From Fig. 3, it is clearly seen that the proposed JP-MAP reconstruction method results in improved bias levels while effectively controlling noise levels.

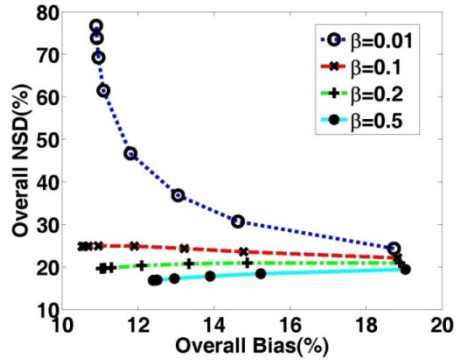

Fig. 2. Plots of overall NSD versus bias curves of brain image changing with the iteration number (1, 2, 3, 5, 10, 15, 20 and 25 (16 subsets)), using JP-MAP with fixed δ and η for varying parameter β.

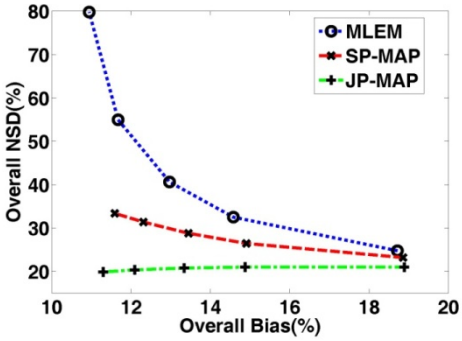

Fig. 3. Plots of overall NSD (noise) versus Bias curves of reconstructed brain images changing with the iteration number (1, 2, 3, 5 and 10 (16 subsets)), using: (i) MLEM, (ii) SP-MAP, and (iii) JP-MAP.

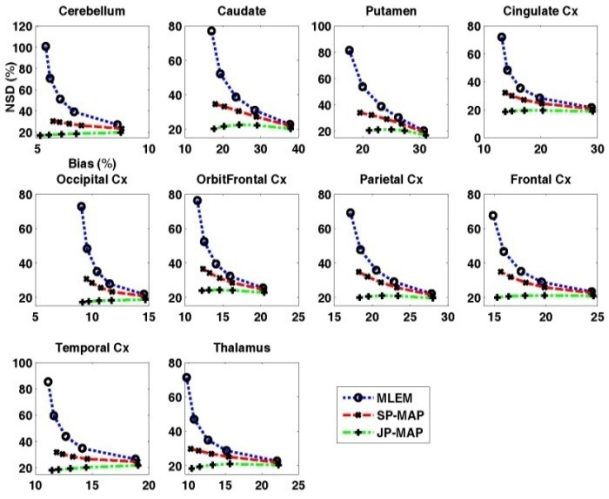

Fig. 4. Plots of regional NSD versus Bias trade-off curves of reconstructed brain images changing with the iteration number (1, 2, 3, 5 and 10 (16 subsets)) for different regions, using (i) MLEM, (ii) SP-MAP, and (iii) JP-MAP.

As depicted in Fig. 4 for the individual ROIs, Noise versus bias tradeoff curves achieved by the proposed JP-

MAP reconstruction method is seen to outperform those from MLEM and conventional MAP.

In order to provide a more direct visual impression of the reconstructed images, Fig. 5 shows transaxial, coronal, and sagittal slices through the reference image as well as images obtained by the three reconstruction algorithms (MLEM, SP-MAP, JP-MAP) with 10 iterations (16 subsets).

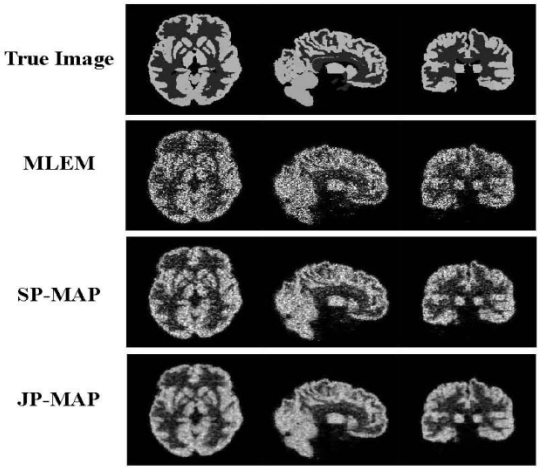

Fig. 5. True and reconstructed images. From top to bottom: (i) true image, (ii) MLEM and (iii) SP-MAP and (iv) JP-MAP. (From left to right): corresponding to transaxial, sagittal and coronal slices, respectively.

5. SUMMARY

This work proposed an OSL MAP reconstruction method for PET brain imaging to enhance the image reconstruction via introduction of joint priors between anatomical and functional image. We adapted a hyperbolic potential function to incorporating the anatomical information and constructed an anatomy-dependent potential function in the joint prior term. Using realistic simulated short time ^{18}FDG PET data, we optimize the performance of the proposed JP-MAP PET reconstruction algorithm, and compared its performance with conventional 3D MLEM and SP-MAP reconstruction algorithms. The proposed JP-MAP reconstruction algorithm resulted in quantitatively enhanced reconstructed images, as demonstrated in extensive ^{18}FDG PET simulation study.

6. REFERENCES

[1] A. Rahmim and H. Zaidi, "PET versus SPECT: strengths, limitations and challenges," *Nucl. Med. Commun.,* vol. 29, pp. 193-207, 2008.

[2] B. Bai, Q. Li and R. M. Leahy, "Magnetic Resonance-Guided Positron Emission Tomography Image Reconstruction," *Semin. Nucl. Med.*, vol. 43, pp. 30-44, 2013.

[3] A. M. Alessio, P. M. Kinahan and T. Lewellen, "Improved quantitation for PET/CT image reconstruction with system modeling and anatomical priors," *Med. Phys.*, vol 33, pp. 695-703, 2005.

[4] B. Lipinski, H. Herzog, E. Rota Kops, W. Oberschelp, and H. W. Muller-Gartner, "Expectation maximization reconstruction of positron emission tomography images using anatomical magnetic resonance information," *IEEE Trans. Med. Imaging.,* vol. 16, pp. 129-136, 1997.

[5] J. E. Bowsher, H. Yuan, L. W. Hedlund, T. G. Turkington, G. Akabani, A. Badea, W. C. Kurylo, C. T. Wheeler, G. P. Cofer, and M. W. Dewhirst, "Utilizing MRI information to estimate F18-FDG distributions in rat flank tumors," *IEEE Nuclear Science Symp. Conf. Record*, pp. 2488-2492, 2004.

[6] K. Vunckx, A. Atre, K. Baete, A. Reilhac, C. M. Deroose, K. Van Laere, and J. Nuyts, "Evaluation of three MRI-based anatomical priors for quantitative PET brain imaging," *IEEE Trans. Med. Imaging,* vol. 31, pp. 599-612, 2012.

[7] D. Kazantsev, A. Bousse, S. Pedemonte, S. R. Arridge, B. F. Hutton, and S. Ourselin, "Edge preserving Bowsher prior with nonlocal weighting for 3D SPECT reconstruction," *IEEE Int. Symp. Biomed. Imaging,* 2011, pp. 1158-1161, 2011.

[8] A. Bousse, S. Pedemonte, D. Kazantsev, S. Ourselin, S. Arridge, and B. F. Hutton, "Weighted MRI-Based bowsher priors for SPECT brain image reconstruction," *IEEE Nuclear Science Symp. Conf. Record*, pp. 3519-3522, 2011.

[9] J. Nuyts, "The use of mutual information and joint entropy for anatomical priors in emission tomography," *IEEE Nuclear Science Symp. Conf. Record*, pp. 4149-4154, 2007.

[10] J. Tang and A. Rahmim, "Bayesian PET image reconstruction incorporating anato-functional joint entropy," *Physics in medicine and biology,* vol. 54, p. 3741-3745, 2009.

[11] S. Somayajula, C. Panagiotou, A. Rangarajan, Q. Li, S. R. Arridge, and R. M. Leahy, "PET image reconstruction using information theoretic anatomical priors," *IEEE Trans. Med. Imaging,* vol. 30, pp. 537-549, 2011.

[12] L. Lu, J. Ma, J. Huang, H. Zhang, Z. Bian, W. Chen, and Z. Liang, "Generalized metrics induced anatomical prior for MAP PET image reconstruction," *Proc. Int. Meeting on Fully 3D Image Recon. in Rad. and Nucl. Med.*, pp. 233-236, 2011.

[13] S. Geman and D. Geman, "Stochastic relaxation, Gibbs distributions, and the Bayesian restoration of images," IEEE Trans. Pattern Anal. Mach. Intell., vol, 13, pp. 721-741, 1984.

[14] P. J. Green, "Bayesian reconstructions from emission tomography data using a modified EM algorithm," *IEEE Trans. Med. Imaging,* vol. 9, pp. 84-93, 1990.

[15] V. Sossi, H. W. de Jong, W. C. Barker, P. Bloomfield, Z. Burbar, M. Camborde, C. Comtat, L. A. Eriksson, S. Houle, and D. Keator, "The second generation HRRT-a multi-centre scanner performance investigation," *IEEE Nuclear Science Symp. Conf. Record,* pp. 2195-2199, 2005.

[16] A. Rahmim, K. Dinelle, J. Cheng, M. A. Shilov, W. P. Segars, S. C. Lidstone, S. Blinder, O. G. Rousset, H. Vajihollahi, and B. Tsui, "Accurate event-driven motion compensation in high-resolution pet incorporating scattered and random events," *IEEE Trans. Med. Imaging,* vol. 27, pp. 1018-1033, 2008.

[17] L. Lu, N. A. Karakatsanis, J. Tang, W. Chen, and A. Rahmim, "3.5 D dynamic PET image reconstruction incorporating kinetics-based clusters," *Physics in Medicine and Biology,* vol. 57, p. 5035-5055, 2012.